Supplementary Information

Luis E. Botello,[a] Marco Schönig,*[b,c] José Solla-Gullón,[a] Víctor Climent,[a] Juan M. Feliu[a] and Rolf Schuster[b]

[a]Instituto Universitario de Electroquimica, Universidad de Alicante, E-03690 Alicante, Spain.
[b]Leiden Insitute of Chemistry, Leiden University, 2300 RA Leiden, The Netherlands. Tel: +31 71 527 2727; *E-mail: m.schonig@lic.leidenuniv.nl
[c]Insitut für physikalische Chemie, Karlsruhe Insitute of Technology, 76131 Karslruhe, Germany.

S1 Determination of $s(\mathrm{H_{ad}})$

As explained already in the main text the electrochemical microcalorimetry determines the heat exchanged at the working electrode. More details about the experimental setup can be found e.g. in ref. 1. The reaction entropy can be derived from the reversibly exchanged, molar heat, *i. e.*, the Peltier heat, after correcting for the transport entropy[2]. In the case of 0.1 M H_2SO_4 the transport entropy amounts to $35.8\,\mathrm{J\,mol^{-1}\,K^{-1}}$ (calculation shown in more detail in the supplementary information of ref. 2).

The reaction entropy in the experimentally investigated potential region between 0.1 V and 0.35 V should correspond to the adsorption process $H^+_{aq} + e^- \rightarrow H_{ad}$ and the double-layer charging. As we expect negligible influence of the pure double-layer charging on the calorimetric measurements at potentials apart from the pzc[3], we allocate the whole measured reaction entropy to the adsorption process. The entropy of the adsorbed proton can be derived by

$$s(H_{ad}) = \Delta_R S - s(e^-) - s(H^+_{aq}) \quad . \tag{1}$$

Since $s(e^-) \approx 0$[4], this leaves only the partial molar entropy of the proton in solution. Using the absolute molar entropy of protons of $-22.2\,\mathrm{J\,mol^{-1}\,K^{-1}}$ listed by Marcus[5], the activity of the proton calculated with the software PhreeQC,[6] and its negligible temperature dependence[7], we directly obtain the molar entropy of the adsorbed hydrogen by using the equation[7]:

$$s_i = s_i^0 - R \cdot \ln a_i - RT \cdot \frac{\partial \ln a_i}{\partial T} \tag{2}$$

The same procedure can be applied to the data using the electrocapillary equation as as outlined in ref. 8 and should lead to the same thermodynamic quantity.

S2 Electrochemical cleaning procedure

When working with non-glass equipment and small solution amounts, as in the present contribution, it is particularly hard to prevent organic impurities from the environment. While the initial setup can be thoroughly cleaned using caroic acid and boiling in ultrapure water, to get rid of basically every metal contaminant as well as most organic impurities, the smallest contact to air can lead to organic contaminants, which will eventually reach and adsorb on the surface[9]. It is therefore imperative, when the solution reservoir is not big enough to stall this effect from happening on the time scale of the experiment or when the experiment takes several hours- to frequently remove these organic contaminants. For polycrystalline electrodes typically electrochemical cleaning is applied, *i. e.*, the electrode potential is swept between the onset of the hydrogen and oxygen evolution, whereupon all organic contaminants will be oxidized, and a constant voltammetric profile is obtained[9]. However, this procedure will lead to severe surface roughening and is therefore not suitable for single-crystals, as well as shape-controlled nanoparticles (NPs). Pt single-crystals used in the hanging-meniscus configuration can be flame-annealed several times over the course of one experiment, resulting in a fresh, clean and ordered Pt surface every time. The effect of the contamination and the commonly used electrochemical cleaning procedure is shown for the spherical nanoparticles in 0.1 M H_2SO_4 in Fig. S1. The CV (lower panel) and reaction entropy (upper panel) for the initial surface state (iteration 1) are shown in black (further discussion of the voltammetric profile can be found in the main text). For each further iteration (grey), we performed potential pulse measurements at the same rest potential, indicated by the dashed blue line, followed by a cyclic voltammogram between 0.05 V and 0.55 V, resulting in a procedure taking several minutes. After 8 iterations of this procedure, we cycled the potential 35 times between 0 V and 1.2 V to obtain a comparable surface state (blue, iteration 9) to the first iteration (black). As apparent from the decrease of the voltammetric response in the hydrogen region between iteration 1 and 8 (grey) the surface was covered by some organic contaminant, resulting in a diminishing hydrogen adsorption current. Parallel to the diminishing current also the reaction entropy decreases between every iteration, leading to a maximum decrease of $4\,\mathrm{J\,mol^{-1}\,K^{-1}}$. After recovery of the initial surface state, the reaction entropy also recovers its initial value. Note that we typically estimate the systematical error resulting from the reconstruction of the heat flux, the calibration procedure and the linear fit of the molar heat to around $2\,\mathrm{kJ\,mol^{-1}}$, which would correspond to $7\,\mathrm{J\,mol^{-1}\,K^{-1}}$. It is clearly evident from Fig. S1, that the statistical error in one experiment is lower than this value and the microcalorimetry is therefore sensitive enough to quantify even minute changes of the surface state of adsorbates.

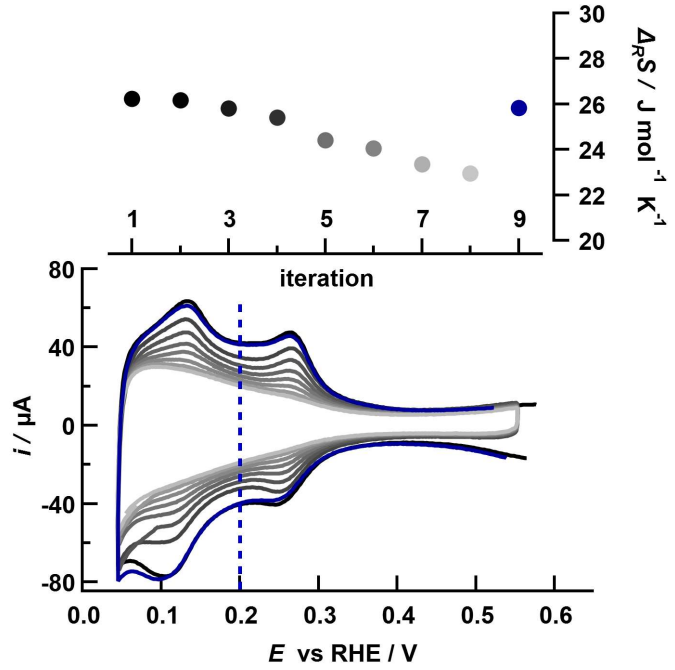

Fig. S1 Upper Panel: Diminishing of the reaction entropy at 0.2 V as a function of potential pulse iterations (black to grey). In the lower panel the diminishing current in the CV is shown (black to grey). After intense electrochemical cleaning the initial values are recovered (blue, both panels).

However, since in this contribution we were interested in the electrochemical response of different shape-controlled nanoparticles, which would lose, at least partially, their shape and ordered domains upon the electrochemical cleaning, this cleaning procedure was not applicable. Besides that, the working electrode could not be disassembled during one experiment, precluding the replacement of the sample with new particles. Finally, the thermal treatment was also precluded since it would alter the size and shape of the NPs. Therefore, we developed a new procedure presented in the experimental section of the main text, through which we expect the hydrogen produced at the surface and the generated highly alkaline local conditions to remove the possible contaminants. The effectiveness of the employed cleaning procedure is shown in Fig. S2. The Figure displays the CV before a set of potential pulses (black), as described in the main text, at the end of a set of potential pulses (light grey) and after the hydrogen cleaning (dark grey). Additionally, the reaction entropy at two different rest potentials is shown, where the values indicated with black and dark grey, were obtained at the beginning of a set of potential pulses, while the light grey value was obtained later in one set of pulses. It is clearly evident, that although the current in the voltammetric profile, especially the current attributed to the adsorption on {110} steps, decreases, the overall geometry of the NPs stays intact. The retaining of the complete (anodic) voltammetric current after the hydrogen cleaning further shows that the employed cleaning method is adequate to regain the initial state of the surface. Upon comparison of the reaction entropy values, we evidence the same effect, namely the initial value is retained at both depicted rest potentials. As already pointed out in the discussion of Fig. S1 this not only shows how sensitive the microcalorimetric method is, but also emphasizes that the methodology employed ensures that the trends in the measured entropy are not due to spurious contaminations.

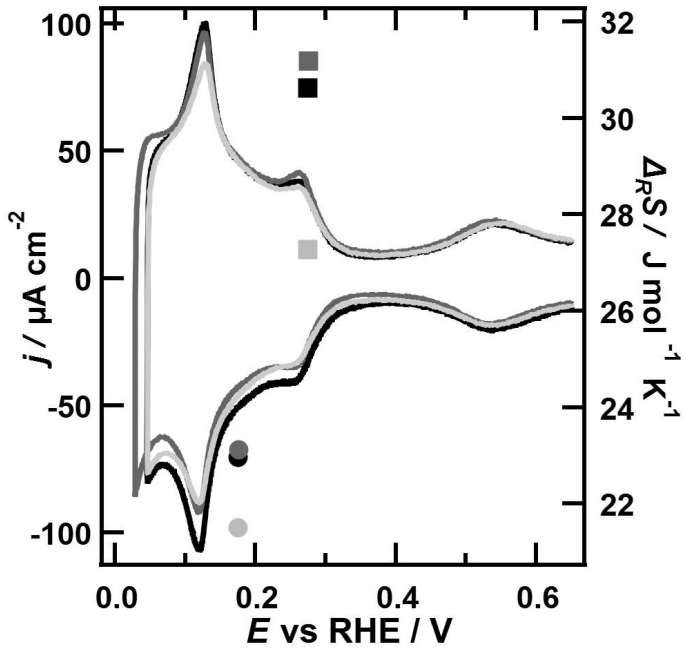

Fig. S2 Effect of the hydrogen cleaning method at two different potentials: The entropy before a set of potential pulses (black), after a set of potential pulses (light grey) and after hydrogen cleaning (dark grey) is shown.

S3 Comparison with the stepped Pt(554) single crystal

The octahedral nanoparticles have extended {111} terraces, which makes them suitable as a model catalyst with behaviour similar to this basal plane. However, there is also a non-negligible contribution from low coordinated atoms at edges of the faces. Therefore, it is even more accurate to make a comparison with a stepped platinum surface. A measured cyclic voltammetry of a Pt(554)=Pt(S)[9(111) × (110)] single crystal electrode is shown on Fig. S3. The profile is quite similar to the one shown in Fig. 1B, however, the peaks from the {110} adsorption contribution are sharper and the current from sulfate adsorption is higher. These differences are reasonable considering that the single crystal electrode contain preferentially monoatomic one dimensional step lines of well defined geometry and long terraces, ideally infinite, in the direction parallel to the step. On the other hand, the nanoparticles contain a broader variability of step geometries and shorter terrace length in both directions. Nevertheless, these are small differences and the electrochemical behavior is expected to be quite similar. It is therefore reasonable to use the octahedral nanoparticles as model for the Pt(554) surface, making the approximation that the adsorption behavior of hydrogen from the solution will be equivalent in terms of the kinetic and thermodynamic properties of the reaction.

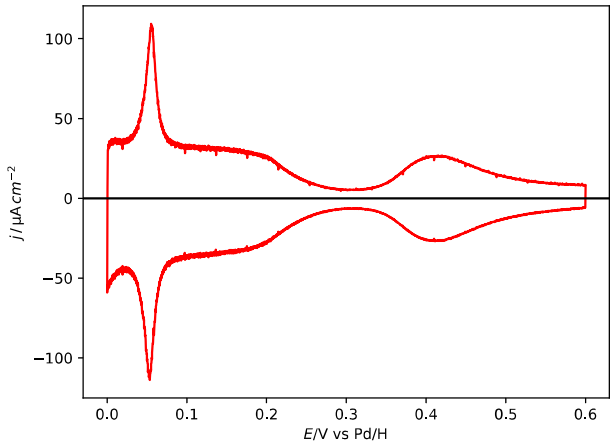

Fig. S3 Cyclic voltammetry of a single crystal Pt(554) electrode at a scan rate of $50\,\mathrm{mV\,s^{-1}}$ in $0.1\,\mathrm{M}$ H_2SO_4.

S4 Contributions of the Au support

As pointed out in the main text, it is necessary to distinguish the heat and current responses of the underlying gold substrate from the response of the Pt NPs. For this purpose, we measured the voltammetric profile of the gold substrate with and without the addition of cubic NPs as shown in Fig. S4. It is readily visible that the current of the sample without the addition of NPs (yellow) is at least 10 times smaller than after the addition of the NPs (black). This implies that upon polarization of the electrode during the calorimetric measurements, mainly the reactions on the NPs will be driven.

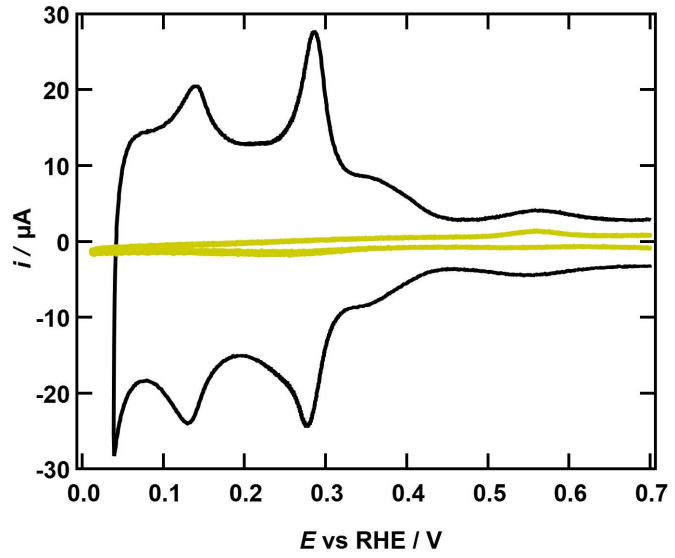

Fig. S4 Cyclic voltammetry of the gold support with (black) and without (yellow) Cubic Pt-NPs in $0.1\,\mathrm{M}$; scanspeed $50\,\mathrm{mV\,s^{-1}}$.

To corroborate this assumption, we also conducted calorimetric measurements on the gold substrate with and without NPs, which are displayed in Fig. S5. As visible from Fig. S5a upon application of a $10\,\mathrm{ms}$, $100\,\mathrm{mV}$ potential pulse, the current drops sharply and levels off immediately as expected for double-layer charging. During the pulse only a negligible temperature change of 0.004 is detected. On the contrary, as visible from Fig. S5b, the application of a $10\,\mathrm{ms}$, $100\,\mathrm{mV}$ potential pulse leads to a sharp, initial current decrease followed by a exponentially decaying current during the complete $10\,\mathrm{ms}$ pulse duration. Moreover, the electrode cools significantly ($\Delta T > 0.25$) during the potential pulse. This clearly shows, that the heat and current response of the gold sample are negligible in comparison with the Pt NPs.

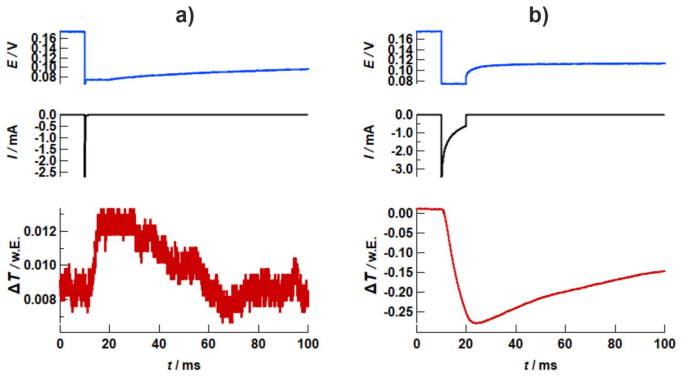

Fig. S5 Potential E (blue), current I (black) and temperature Δ T (red) transients, resulting from a $10\,\mathrm{ms}$, $-100\,\mathrm{mV}$potential pulse starting at $0.18\,\mathrm{V}$ on a) Au(111) and b) Au(111) covered with octrahedral NPs in $0.1\,\mathrm{M}$ H_2SO_4.

S5 Influence of the Electrolyte anion

To clarify, whether there is a significant influence of the electrolyte anion on the entropy of the adsorbed hydrogen, we investigated solutions containing the non-specifically adsorbing ClO_4^- and the specifically adsorbing SO_4^{2-}. The obtained CVs and the entropy of the adsorbed hydrogen from $0.1\,\mathrm{M}$ H_2SO_4 and $0.1\,\mathrm{M}$ $HClO_4$ on the octahedral NPs are shown in Fig. S6. The difference between both anions is especially evident in the voltammetric response in the potential region between $0.45\,\mathrm{V}$ and $0.65\,\mathrm{V}$, where in H_2SO_4 a current wave originating from the specific adsorption of SO_4^{2-} is visible. It is further visible that although the current wave corresponding to hydrogen adsorption in the voltammetric profile in $HClO_4$ is less pronounced, which is a trait also observed on single-crystal electrodes [10], the entropy of the adsorbed hydrogen is basically not affected by the electrolyte anion.

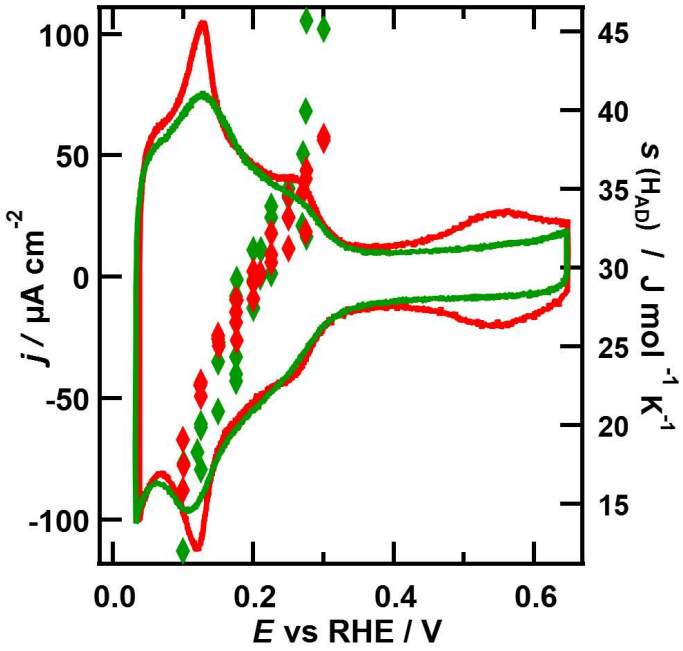

Fig. S6 CV and entropy of adsorbed hydrogen on octahedral NPs in 0.1 M H_2SO_4 (red) and 0.1 M $HClO_4$ (green) solution.

S6 Nanoparticle morphology

A representative image of each kind of the shape controlled nanoparticles can be observed in Fig. S7. The surface of the nanoparticles presents many more features compared to the single crystal surface they are compared to, including different steps, corners, kinks and edges, which make them a more complex system. However, the high control of the 3D geometry of the particles allows for the dominance of oriented terraces regarding the electrochemical behavior as described in the main text.

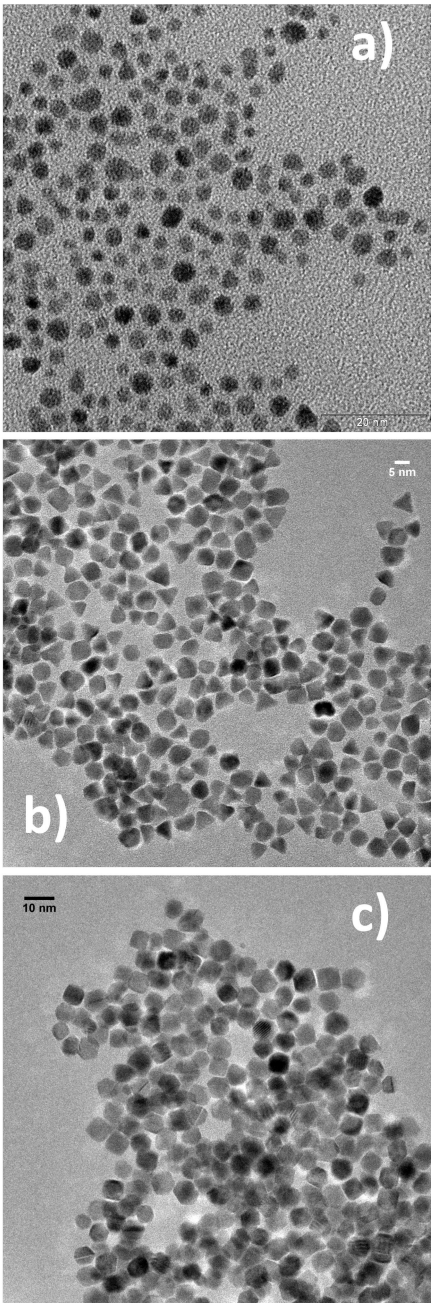

Fig. S7 Representative TEM image of a) spherical, b) octahedral and c) cubic nanoparticles.

Notes and references

1 S. Frittmann, V. Halka, C. Jaramillo and R. Schuster, *Review of Scientific Instruments*, 2015, **86**, 064102.

2 M. Schönig, S. Frittmann and R. Schuster, *ChemPhysChem*, 2022, **23**, e202200227.

3 M. Schönig and R. Schuster, *Physical Chemistry Chemical Physics*, 2023, **25**, 5948–5954.

4 B. E. Conway, H. Angerstein-Kozlowska and W. B. A. Sharp, *Journal of the Chemical Society, Faraday Transactions 1*, 1978, **74**, 1373–1389.

5 Y. Marcus, *Ion solvation*, Wiley, Chichester, 1985.

6 D. L. Parkhurst and C. A. J. Appelo, *Description of input and examples for PHREEQC version 3–A computer program for speciation, batch-reaction, one-dimensional transport, and inverse geochemical calculations*, 2013.

7 N. García-Araez, V. Climent and J. M. Feliu, *Journal of Solid State Electrochemistry*, 2008, **12**, 387–398.

8 N. García-Araez, V. Climent and J. M. Feliu, *The Journal of Physical Chemistry C*, 2009, **113**, 19913–19925.

9 B. E. Conway, H. Angerstein-Kozlowska, W. B. A. Sharp and E. E. Criddle, *Analytical Chemistry*, 1973, **45**, 1331–1336.

10 C. Korzeniewski, V. Climent and J. M. Feliu, *Electroanalytical Chemistry: A Series of Advances*, 2012, vol. 24, pp. 75–169.